The Journal of Membrane Biology (2019) 252:343–356
https://doi.org/10.1007/s00232-019-00074-5

Revealing a Dual Role of Ganglioside Lipids in the Aggregation of Membrane-Associated Islet Amyloid Polypeptide

Mikkel Christensen[1,2] · **Birgit Schiøtt**[1]

Received: 21 January 2019 / Accepted: 9 June 2019 / Published online: 20 June 2019

Abstract

Amyloid formation of the human islet amyloid polypeptide (hIAPP) correlates with a loss of insulin-producing beta cells in patients with type II diabetes mellitus. In this study, we investigated the binding of hIAPP to bilayers consisting of ganglioside lipids and dioleoylphosphatidylcholine (DOPC), which is a physiologically relevant lipid species for pancreatic beta cell-associated aggregation. The membrane interactions are studied computationally using a combination of coarse-grained, umbrella sampling, and atomistic molecular dynamics simulations. Herein, we demonstrate how the hIAPP peptides accumulate in the areas with a high content of ganglioside lipids. We have characterized two distinct binding modes of hIAPP on ganglioside-rich membranes, with both binding modes formed due to electrostatic interaction between the cationic peptides and the anionic ganglioside headgroup. We observed that binding in the ganglioside headgroup region induced conformational changes of the peptide towards an aggregation prone conformation, rich in β-strands. In contrast, the binding of hIAPP near the ganglioside-enriched areas mobilizes the peptide, preventing it from conformational changes and potentially shields it from interactions with other peptides. This suggests a dual role of ganglioside lipids, affecting the aggregation of hIAPP by either accelerating or inhibiting amyloid formation depending on the membrane binding and the ganglioside concentration.

Graphic Abstract

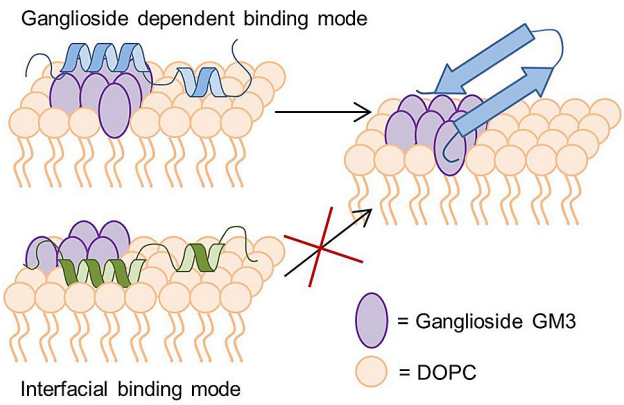

Keywords Amyloid · Lipid membranes · Misfolding · Diabetes · Aggregation

Introduction

Amyloid deposits play a role in a wide range of diseases, including Parkinson's disease, Alzheimer's disease, and type II diabetes mellitus (T2DM). In T2DM, the major constituent of amyloid fibrils deposited in the pancreas is the peptide hormone called human islet amyloid polypeptide (hIAPP,

Electronic supplementary material The online version of this article (https://doi.org/10.1007/s00232-019-00074-5) contains supplementary material, which is available to authorized users.

✉ Birgit Schiøtt
birgit@chem.au.dk

Extended author information available on the last page of the article

also commonly known as amylin) (Maloy et al. 1981; Westermark 1995). In response to elevated blood sugar, the pancreatic beta cells secrete hIAPP and insulin, as a physiological signal to decrease the glucose level in the blood (Lukinius et al. 1989). The signaling pathway of hIAPP is unclear; however, it signals the inhibition of glucagon secretion, gastric emptying, and food intake (Lutz 2012). Insulin signals for the liver, muscle, and adipose tissue to take up and process glucose from the blood (Wilcox 2005). A decreased response to insulin is a hallmark of T2DM, and the initial cause of hyperglycemia (Wilcox 2005). The amyloid formation of hIAPP correlates with a loss of beta cells (Höppener et al. 2000; Jurgens et al. 2011), leading to a decreased production of insulin and hIAPP to regulate glucose metabolism (Stumvoll et al. 2007; Westermark et al. 2011; Zhao et al. 2003). The loss of beta cells attributes is attributed to the cytotoxicity of hIAPP aggregates; however, the mechanism of cytotoxicity is unclear. Cryo-TEM imaging (Engel et al. 2008) and confocal fluorescence microscopy (Sparr et al. 2004) have revealed that pre-formed fibrils leave vesicles intact, while the presence of hIAPP fibril seeds leads to a distortion of vesicles, this indicates that the growth process of amyloid fibrils is the reason for the cytotoxicity. Based on observations from AFM (Quist et al. 2005), electrochemical measurements (Mirzabekov et al. 1996), as well as leakage of content from lipid vesicle (Anguiano et al. 2002; Engel et al. 2008; Last et al. 2011; Scalisi et al. 2010), studies have indicated that oligomer structures of hIAPP can penetrate lipid membranes and form non-selective ion channels and thereby induce cell death.

Fig. 1 The primary structure of hIAPP. The molecular formula of the terminals is indicated at the ends of the sequence. The *N*-terminal, Lys1, and Arg11 are shown in blue, since they are expected to be positively charged at physiological pH and will be treated as such in this study (Color figure online)

hIAPP consists of 37 residues, with the sequence shown in Fig. 1. At physiological pH it carries a +3e charge; from the *N*-terminal, Lys1 and Arg11. The *C*-terminus is physiologically amidated and is therefore neutral. Furthermore, His18 can be protonated to become cationic depending on the environment. A disulfide bridge connects Cys2 and Cys7.

The hIAPP is an intrinsically disordered peptide, meaning that monomeric hIAPP does not take a unique-folded structure in solution, but is unfolded, i.e., alternates between different structures as reported by nuclear magnetic resonance (NMR) spectroscopy (Williamson et al. 2009; Williamson and Miranker 2007), circular dichroism (CD) spectroscopy (Williamson et al. 2009), and conformational ensembles from MD simulations (Hoffmann et al. 2015). Attached to lipid membranes and in membrane-mimicking environments (such as SDS micelles), hIAPP forms stable α-helical conformations prior to converting into amyloid fibrils. This process has been followed using CD spectroscopy and vibrational sum frequency generation (Caillon et al. 2013; Fu et al. 2015; Knight et al. 2006, 2008). Structural ensembles of hIAPP in complex with sodium dodecyl sulfate (SDS) micelles have been determined using constraints from solution-state NMR spectroscopy: The structural ensembles solved at pH 7.4 with all the physiological chemical modifications show α-helical conformations with a kink around residue Ser20 (Fig. 2a) (Nanga et al. 2011). A β-hairpin conformation of monomeric hIAPP is observed on the pathway to amyloid formation from MD simulations (Reddy et al. 2010; Singh et al. 2013), NMR spectroscopy of β-wrap protein binder (Mirecka et al. 2016), and ion-mobility spectrometry-mass spectrometry (Dupuis et al. 2011). The β-hairpin conformation has a turn and β-strand

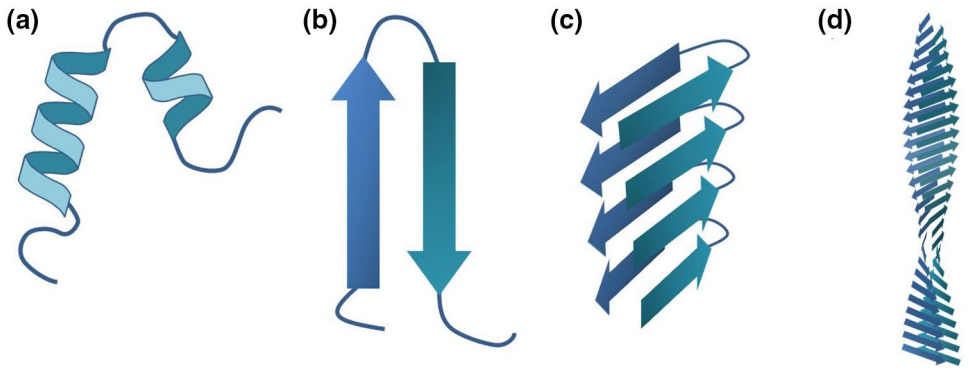

Fig. 2 Sketches of hIAPP structures inspired by experimental results. **a** An α-helical conformation from the NMR ensemble (pdb-id 2L86) (Nanga et al. 2011). **b** Hairpin structure of hIAPP, a proposed pre-nuclear structure (Dupuis et al. 2011; Reddy et al. 2010; Singh et al. 2013). **c** Fraction of hIAPP fibril structure (Luca et al. 2007). **d** Extended structure of a hIAPP amyloid fibril (Luca et al. 2007)

in the same segments as the currently available structures of mature hIAPP fibrils (Fig. 2b) (Dupuis et al. 2011; Reddy et al. 2010; Singh et al. 2013). Structures of mature amyloid fibrils of hIAPP have been determined using solid-state NMR. The fibril structure consists of stacked β-hairpin with a turn in the segment of residue His18 to Phe23 (Fig. 2c) (Luca et al. 2007). The β-strands connect adjacent peptides resulting in long-twisted fibrils with two parallel β-sheets (Luca et al. 2007). Figure 2d shows a schematic of an amyloid fibril.

It is known that lipid membranes affect the aggregation rate of hIAPP (Jayasinghe and Langen 2007). Often the membrane-associated aggregation process is studied in vitro in phospholipid vesicles with zwitterionic phosphatidylcholine (PC) lipids and anionic phospholipids such as phosphatidylserine (PS) and phosphatidylglycerol (PG). Anionic PS and PG lipids drastically increase the rate of aggregation and membrane perforation of hIAPP; this has been observed from kinetic measurements using CD spectroscopy (Jayasinghe and Langen 2005; Lee et al. 2012), Thioflavin-T (ThT) binding assays (Jayasinghe and Langen 2005; Zhang et al. 2017), and dye-leakage experiments (Lee et al. 2012; Zhang et al. 2017).

However, anionic PS and PG lipids are not present in the outer leaflet of β-cell membranes. A more physiologically relevant type of anionic lipid is ganglioside lipids (G-lipids) (Dotta et al. 1989). G-lipids are glycolipids characterized by a sphingosine tail and a number of sugar residues attached to it. A negatively charged *N*-acetylneuraminic acid (NANA) group is a common element of gangliosides. G-lipids spontaneously form clusters in the membrane (Fujita et al. 2007), regardless of any repulsion between the negatively charged NANA fragments, and thus G-lipids form an anionic environment just above the membrane. In microdomain-forming membranes, G-lipids localize in the liquid-ordered phase (Koldsø et al. 2014). A simple ganglioside lipid is GM3, which consists of a sphingosine base with glucose, galactose, and NANA attached (Fig. 3). More complex G-lipids, such as GM1, are branched with additional sugar residues.

GM3 is a major component of the pancreas (Dotta et al. 1989), and its pancreatic concentration increases with diabetes in rats (Saito et al. 1999). Furthermore, G-lipids together with cholesterol increase the cytotoxicity of hIAPP towards PC12 cells (Wakabayashi and Matsuzaki 2009). Interestingly, single-particle tracking experiments have shown that hIAPP co-localizes with the G-lipids in vitro (Calamai and Pavone 2013).

The interaction between amyloid peptides and G-lipids has previously been investigated for the case of Amyloid-β (Aβ). As GM1 is one of the most abundant G-lipids in the brain, many studies have focused on this lipid species (Mocchetti 2005). Using MD simulations, Manna and Mukhopadhyay (2013) investigated the interactions between Aβ and

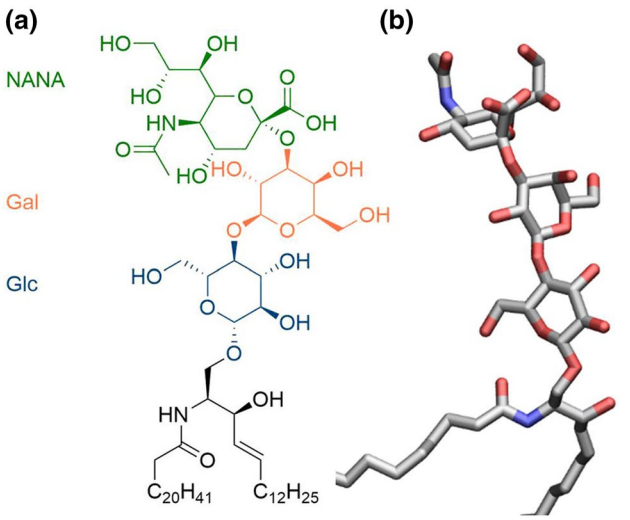

Fig. 3 Ganglioside structure. **a** Structure of GM3 consisting of a sphingosine base with glucose (Glc), galactose (Gal), and *N*-Acetylneuraminic acid (NANA) attached to it. **b** Atomistic representation of GM3

membranes containing 1-palmitoyl-2-oleoyl-sn-glycero-3-phosphocholine (POPC), GM1, and cholesterol. They found that Aβ would bind on the head groups of GM1 aided by CH–π interactions and hydrogen bonding between the peptides and the ganglioside head groups. They also hypothesized that GM1 induces the transition of Aβ to β-hairpin structures considered to be on the pathway to fibril formation. Similar observations were made in other studies of comparable systems with Aβ and GM1 (Lemkul and Bevan 2011), also using MD simulations. Aβ and IAPP have very similar properties with regard to membrane interactions, and both peptides adopt an α-helical conformation when interacting with lipid membranes prior to amyloid formation (Terzi et al. 1997; Wahlström et al. 2008). Recently, Amaro et al. investigated the amyloid formation of Aβ using Z-scan fluorescence spectroscopy, cross-correlation spectroscopy, fluorescence lifetime Förster resonance energy transfer, and MD simulations (Amaro et al. 2016). They found that in membranes containing DOPC, cholesterol, sphingomyelin, and 4% GM1, Aβ oligomerization is inhibited, whereas membranes with 20% GM1 accelerated oligomerization.

In this study, we have performed MD simulations to investigate the binding and interactions between monomeric hIAPP and GM3-enriched model membranes. Although various G-lipid species are present in the pancreatic islets (Dotta et al. 1989), for this study GM3, being a simple G-lipid, will serve as model G-lipid. G-lipids are challenging to study using atomistic MD simulations since they are bulky molecules with a slow dynamics. Therefore, we have used a coarse-grained approach to study the initial binding and organization of hIAPP on GM3-containing membranes,

followed by atomistic simulations to refine the peptide conformations and the specific interactions between the peptides and the membrane. The MARTINI coarse-grained model has previously been applied to study ganglioside lipids in the interactions with proteins, and despite the coarse-grained resolution it has showed good agreement with atomistic simulations (Gu et al. 2016; Koldsø et al. 2014; López et al. 2013). We further use coarse-grained simulations in combination with umbrella sampling, to estimate the binding energy of the binding modes. The formation of microdomains could potentially change the interaction between hIAPP and G-lipids. Microdomain-forming membranes would typically include cholesterol, sphingomyelin, glycolipids, and saturated lipids (Laude and Prior 2004). With such complex membranes containing several lipid components, it can be difficult to isolate the effect of the individual lipid types, we have therefore chosen to focus on gangliosides alone in this study.

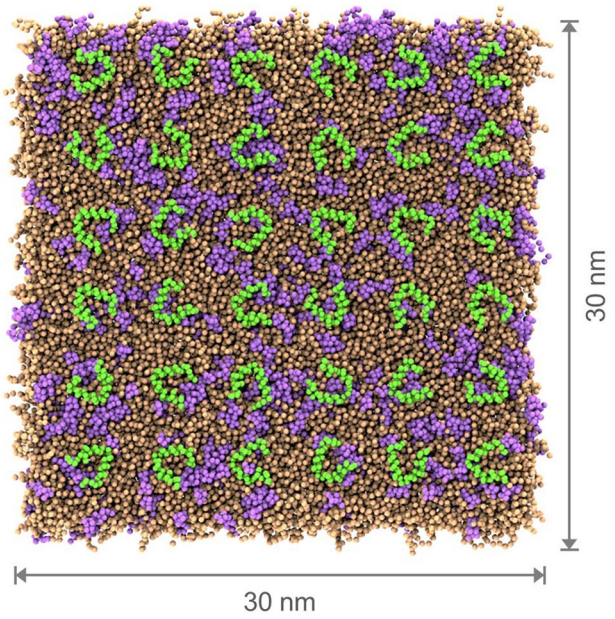

Fig. 4 Simulation setup of the large systems. The system contains a membrane of approximately size 30×30 nm and a composition of 80% DOPC (orange) and 20% GM3 (purple). The 36 peptides of the upper leaflet are shown in green. Water and ions are not shown (Color figure online)

Computational Methods

Here, we present atomistic and coarse-grained MD simulations of hIAPP interacting with DOPC/GM3 membranes. To investigate the binding of hIAPP to DOPC/GM3 membranes, coarse-grained simulations were performed with pre-equilibrated bilayers of approximately 30×30 nm with 20% GM3 in each leaflet and 36 equally spaced peptides placed above each leaflet with a random orientation in the plane of the membrane, as illustrated in Fig. 4. A system of this size will simultaneously allow investigation of lipid organization and provide a large sampling of peptides interacting with the membrane.

Additionally, single-peptide binding simulations were performed in which only one peptide was placed 6 nm above the center of a membrane of approximately size 8×8 nm, as illustrated in Fig. 5. Selected structures from the single-binding simulations were converted to atomistic description using the *Backwards* script (Wassenaar et al. 2014). An overview of the simulations is provided in Table 1.

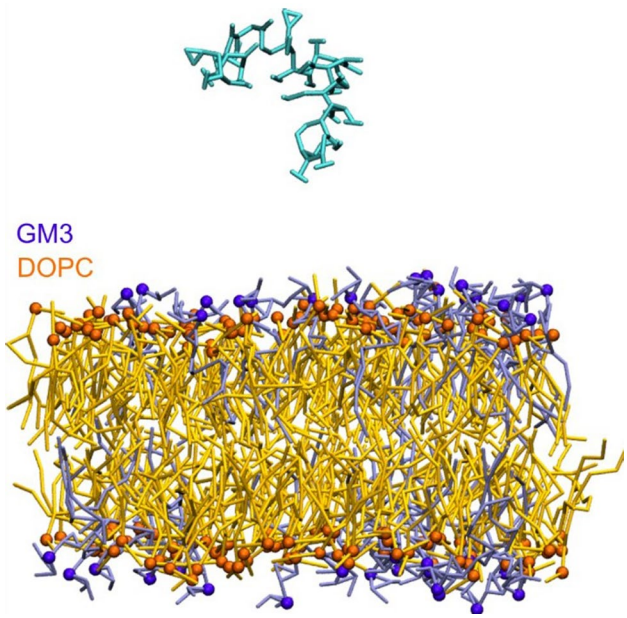

Fig. 5 Setup for single-peptide binding simulations. IAPP is shown cyan, the DOPC lipid in orange, and the ganglioside lipids in purple (Color figure online)

Coarse-Grained Simulations

All simulations were performed with GROMACS 5.1 (Abraham et al. 2015). The hIAPP peptides and waters were modeled with the polarizable MARTINI 2.2P model (de Jong et al. 2013; Yesylevskyy et al. 2010), and the lipids and ions were modeled using MARTINI 2.0 FF (Marrink et al. 2004, 2007). Ions were added for neutralization and to a concentration of 0.15 M. The bilayers were generated with the *Insane* script, which places the lipids randomly within the leaflets in a specified ratio (Wassenaar et al. 2015). The leap-frog integrator (Hockney et al. 1974) was used with a timestep of 20 fs. The peptide structure was based on the lowest energy structure found in the PDB-ID 2L86 (Nanga et al. 2011). It contains a conformational ensemble of SDS micelle-bound

Table 1 Simulation overview

	GM3 conc.	Simulation time	Number of peptides	Membrane dimensions *x*–*y* (nm)	Number of repeats
Large system (CG)	20%	10 µs	72	30×30	5
Single binding (CG)	20%	0.5 µs	1	8×8	100
	4%	0.5 µs	1	8×8	100
Umbrella sampling (CG)	20%	30×0.5 µs	1	8×8	5
Atomistic setup	20%	2 µs	1	8×8	6

IAPP from solution-state NMR. The coarse-grained topology of the peptide was generated using the *Martinize* script. The MARTINI force field has been shown to be to over-aggregate or too "sticky," especially with very hydrophilic molecules such as proteins and saccharides (Javanainen et al. 2017; Schmalhorst et al. 2017). The current GM3 parameters were developed to overcome this artifact and better reproduce the aggregation propensities observed in atomistic simulations, and were therefore employed herein (Gu et al. 2016).

During equilibration, the pressure was controlled using the Berendsen weak coupling algorithm with a τ_P of 12 ps (Berendsen et al. 1984), while in the production runs the Parrinello and Rahman (1981) pressure control with a τ_P of 24 ps was applied. Both during equilibration and production, a compressibility of 3×10^{-4} bar^{-1} was used, and the pressure control was applied semi-isotropically. The temperature was controlled with the velocity rescaling algorithm (Bussi et al. 2007). The electrostatic interactions were described with a reaction field (Tironi et al. 1995) with a cutoff of 1.1 nm. The relative dielectric constant ε_r was set to 2.5 and for the reaction field it was set to infinity. The vdW interactions were modified with a potential shift with a Verlet cutoff scheme (Páll and Hess 2013). Periodic boundary conditions were applied with the neighbor list updated using a Verlet cutoff scheme with a tolerance of 5 $\frac{J}{\text{mol ps}}$.

Atomistic Simulations

Selected structures from the CG single-peptide binding simulations were converted to atomistic resolution using the MARTINI *Backward* script (Wassenaar et al. 2014). The atomistic simulations were performed using GROMACS 5.1 (Abraham et al. 2015). The peptides were modeled with the CHARMM22* FF and the water, ions, and lipids with the CHARMM36 FF. The CHARMM22* FF as proven superior for simulation of intrinsically disordered peptide (Piana et al. 2011) and in simulation of solution-state hIAPP, it samples ensembles of structures in agreement with experimental data (Hoffmann et al. 2015). The leap-frog integrator (Hockney et al. 1974) was used with a time step of 2 fs.

First a short 1-ns equilibration with constant temperature and constant volume (NVT) was performed. For the NVT equilibration, the Velocity rescaling algorithm (Bussi et al. 2007) was used to control the temperature. Following this, a constant pressure, constant temperature equilibration (NPT) of 5 ns was performed prior to production. For the NPT equilibration and production runs, the temperature was held at 310 K using the Nose–Hoover thermostat (Hoover 1985). The pressure was controlled with the Parrinello–Rahman pressure coupling (Parrinello and Rahman 1981) to maintain a pressure of 1 bar. The pressure coupling was applied semi-isotropically with a time constant τ_P of 5 and an isothermal compressibility of 4.5×10^{-5} bar^{-1}. All bonds to hydrogens were constrained with the LINCS algorithm (Hess et al. 1997). A cutoff was applied for the vdW interactions modified with a force-switch function (Steinbach and Brooks 1994) that switches off the interactions between 1.0 and 1.2 nm. For the electrostatic interactions, PME (Essmann et al. 1995) was used with the Verlet cutoff scheme with a 1.2-nm cutoff for the short-range electrostatics.

Results and Discussion

Here, we present atomistic and coarse-grained MD simulations of hIAPP interacting with DOPC/GM3 membranes. An overview of the simulations is provided in Table 1.

To investigate the binding of hIAPP to DOPC/GM3 membranes, large systems were constructed with bilayers of approximately 30×30 nm with 20% GM3 in each leaflet and 36 equally spaced peptides placed away from each leaflet with a random orientation in the plane of the membrane, as illustrated in Fig. 4. With such a large bilayer, it will be possible to observe clustering of the lipids and with 36 peptides it will also provide a platform for a large sampling of membrane-bound peptide conformations. A concentration of 20% GM3 is a high concentration of ganglioside; this concentration was chosen as it compares well with the concentration of anionic lipids in many experimental studies of similar systems (Khemtémourian et al. 2011; Zhang et al. 2017).

Identifying Binding Modes

The distance between the peptides and the hydrophobic–hydrophilic interface of the membrane (defined by the average position of the phospholipid phosphates) in the large systems is shown in Fig. 6a. The distances revealed two distinct binding modes defined by the position of the *N*-terminal α-helix. One mode has the helix close to the hydrophobic–hydrophilic interface, hence termed the interfacial binding mode (I-BM), and the other mode has the helix located at the ganglioside head group region about 6 Å above the interface, this binding mode is referred to as the ganglioside-dependent binding (G-BM). In the following discussion, the binding modes are described using a definition based on the orientation of the *N*-terminal helix (Fig. 6): In G-BM, Ala8, Leu12, and Leu16 are positioned above Glu10 and Glu14 and vice versa for I-BM. The two binding modes are sketched in Fig. 7.

The peptide in the G-BM positions the hydrophilic side of the helix pointing towards the membrane, interacting with the ganglioside headgroups, whereas peptides in the I-BM have the hydrophobic side extending towards the lipid tails (see Figs. 6, 7). The *C*-terminal of the peptide is more flexible and there is no significant difference between the membrane distances of the *C*-terminal residues of the two binding modes. The cationic *N*-terminus and Lys1 are on average positioned at the level of the anionic NANA of the ganglioside head groups in both binding modes. In the large systems, 42% of the peptides where found in G-BM and 42% of peptides positioned as I-BM; the remaining 16% of the peptides did not bind with a clear pattern, and they will not be discussed further herein. The position of the *C*-terminal residues 19–37 is less dependent on the binding mode, although opposite orientation of the *C*-terminal helix is indicated among the two binding modes from the slight saw shape of residues 20 to 30 in Fig. 6a.

Based on the simulations of the large membrane systems, the two binding modes appeared to be occupied with equal likelihood. The large size of these membranes allowed clustering of the ganglioside lipids and thereby allowing the formation of ganglioside-enriched and ganglioside-depleted

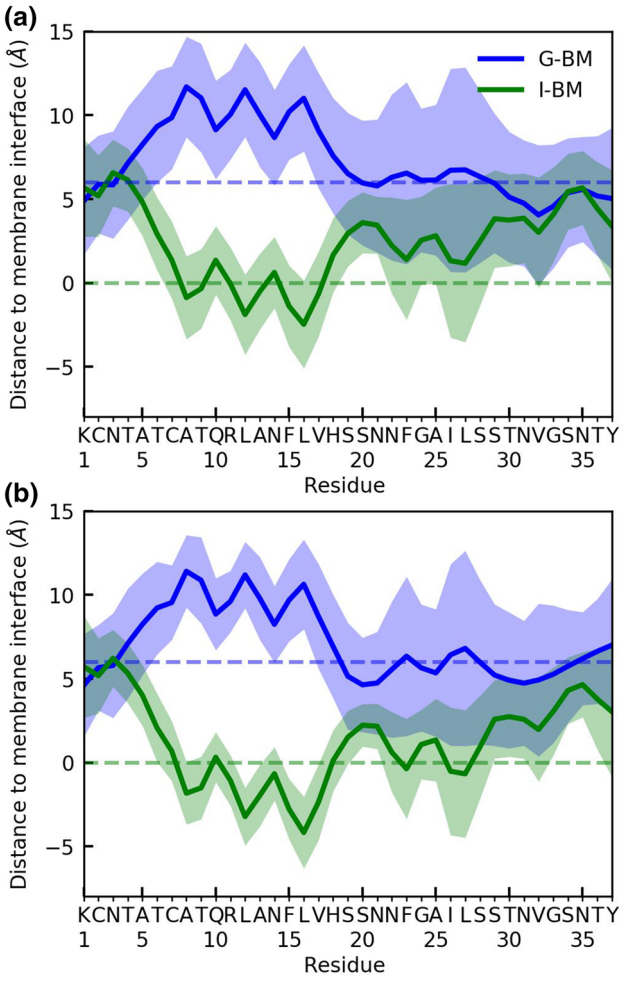

Fig. 6 Average distance from each residue (Cα atom) to the average position of phosphates in the upper leaflet. **a** The 5 repeats for the large systems **b** The 100 single-peptide binding simulations. The average distance of two binding modes (G-BM and I-BM) are shown in blue and green lines, respectively, with the standard deviation indicated by shaded colors. The interface is indicated with a green dashed line, and the average position of the GM3 NANA is indicated with a blue dashed line (Color figure online)

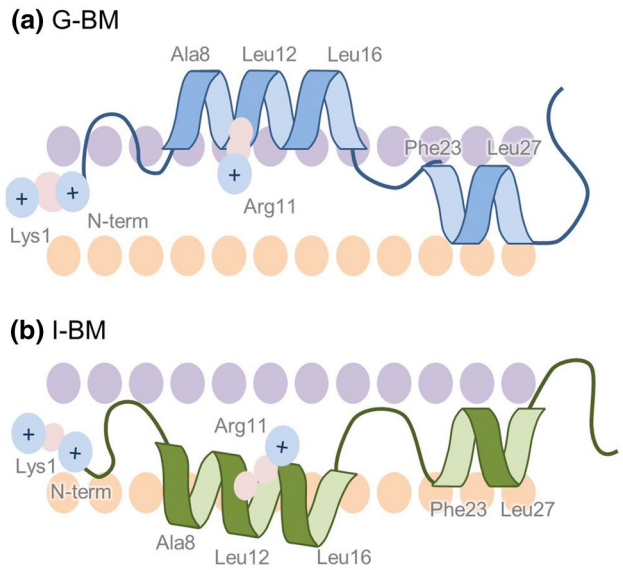

Fig. 7 Binding mode sketch. The peptide in G-BM and I-BM are shown in blue and green, respectively. The position of the anionic bead of NANA is indicated with purple circles and the position of the phospholipid phosphates is illustrated with orange beads. Selected hydrophobic residues are marked, and the cationic residues are depicted with blue (cationic) and pink (other) beads (Color figure online)

areas (Fig. 8). This partitioning might be the cause of the two binding modes, as one binding mode is on top of the ganglioside lipids and the other at the level of the phospholipids.

To investigate the binding without the effect of a large membrane and a large number of peptides, 100 simulations were performed in which only one peptide was included. These simulations were started with a single peptide at 6 nm above the center of a membrane of an approximate size of 8 × 8 nm. Of these, 100 simulations in 34 and 43 the peptides bound to the membrane in G-BM and I-BM, respectively. This supports the hypothesis of the presence of two distinct binding modes, independent of the formation of larger ganglioside-depleted areas and peptide association. The occupancy of the two states remains similar, although indicating a slight preference for I-BM. The residue–membrane distance curves of the single-peptide binding simulations display slightly less fluctuation (Fig. 6b), especially in the *N*-terminal helix region. This decrease could be due to the shorter timescale of the single-peptide simulations compared to the large systems (0.5 µs vs. 10 µs), as well as the absence of possibility of interactions with other peptides could potentially perturb the binding modes slightly by competing interactions between the peptides and the membrane.

At lower GM3 concentration, the likelihood of the peptides binding on the ganglioside headgroups (G-BM) is expected to decrease, and additionally the low concentrations naturally inhibit the clustering of gangliosides. To test this, we performed 100 single-peptide binding simulations

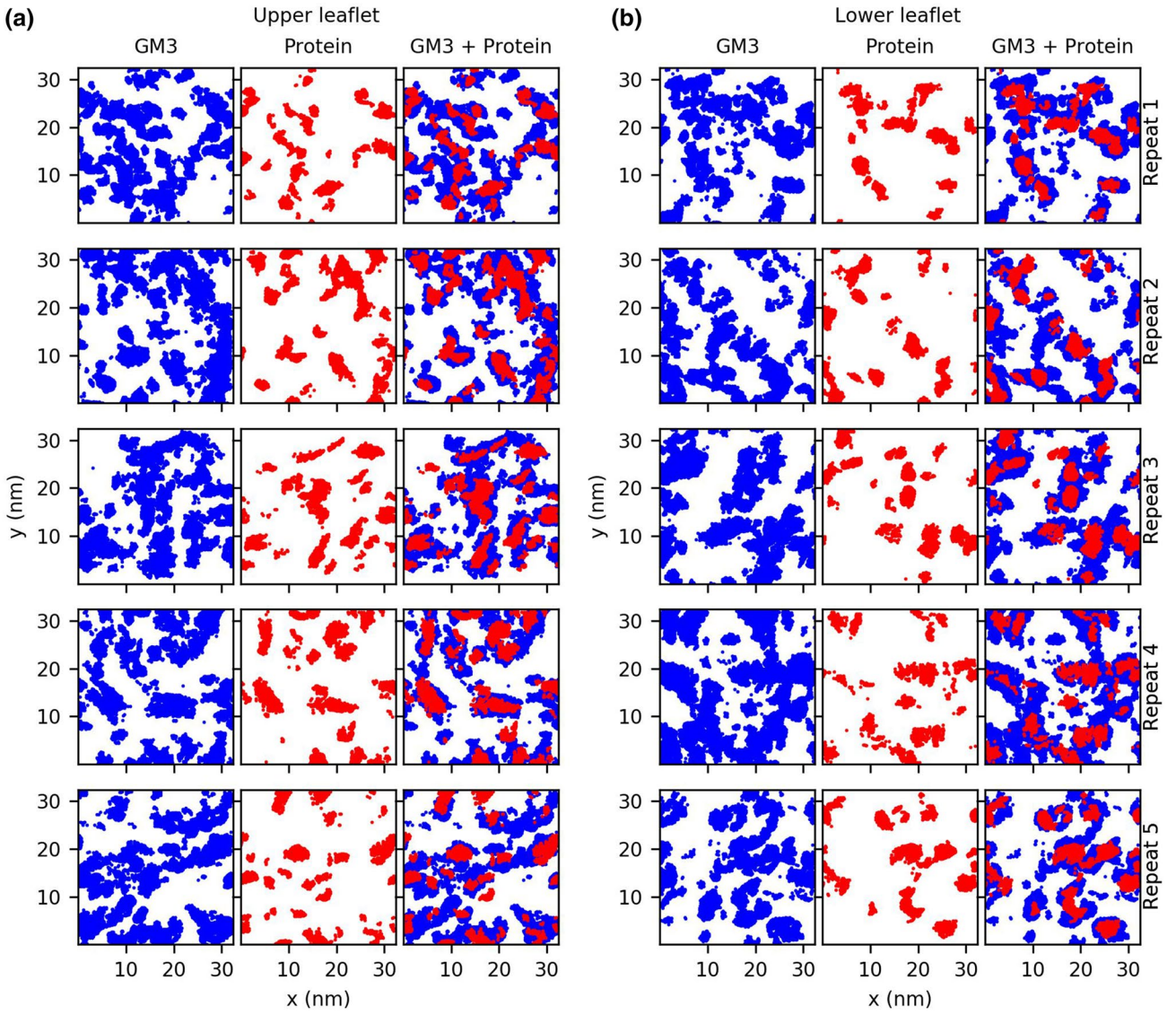

Fig. 8 Areas with the highest density of GM3 (blue) and protein backbone (red) in the last 0.5 µs of 5 repeats of the large system CG simulations for **a** the upper leaflet and **b** the lower leaflet (Color figure online)

with 4% GM3 in the membrane. I-BM was observed for 75% of the peptides and only 7% of the peptides bound in G-BM, thus confirming that G-BM is dependent on a high-ganglioside concentration.

Electrostatic Interactions

hIAPP has a +3e charge (+4e if His18 is found as a histidinium residue) at the *N*-terminal part of the peptide at physiological pH (*N*-terminal, Lys1, and Arg11). Salt-bridge interactions between hIAPP and the anionic elements of the membrane can thus be expected to serve as a driving force towards membrane binding. Numerous studies have shown that anionic lipids accelerate and increase the binding of hIAPP to the membrane (Engel et al. 2008; Sasahara et al. 2010; 2012). HIAPP is thus expected to interact with gangliosides since these are anionic lipids abundant in the pancreatic islets cell membrane,(Dotta et al. 1989) by interacting directly with the negative charge at the NANA. The positively charged elements of hIAPP can alternatively interact with the negative charge at the phosphate group of the zwitterionic phospholipids or be stabilized in the solution by negative ions.

The average fraction of peptides forming each of the possible salt bridges during the last 5 μs of the simulations of the large systems is shown in Fig. 9a. A salt bridge is defined as being present if two beads of opposite charge are within a distance of 7 Å of each other as recommended for the MARTINI force field.(Periole 2013) In the G-BM, Lys1 and the *N*-terminal both interact with PO4 around 50% of the time, and with NANA approximately 70% and 80% of the time, respectively. This indicates that the *N*-terminal is located above or at the level of the ganglioside head groups. Arg11 displays a similar tendency, although less pronounced; it interacts with PO4 approximately 20% of the time and with NANA around 45% of the time. In the I-BM, the interaction of Lys1 and the *N*-terminus with PO4 is present for about 40% of the peptides, whereas the interaction with NANA is present in around 60% of the time.

The most pronounced difference when comparing to G-BM is found for the interaction of Arg11, which interacts with PO4 approximately 70% of the time in the I-BM, but only interacts with NANA in around 20% of the time in this binding mode. In I-BM, the peptides are thereby strongly interacting with the phospholipids through interactions with Arg11.

Again, to account for the effect of ganglioside-depleted and -enriched domains; the results are compared with the results from the single-peptide binding simulations (Fig. 9b). The results are very similar, though with smaller standard deviations for the single-binding simulations. The only major difference is seen in the interaction pattern of Arg11

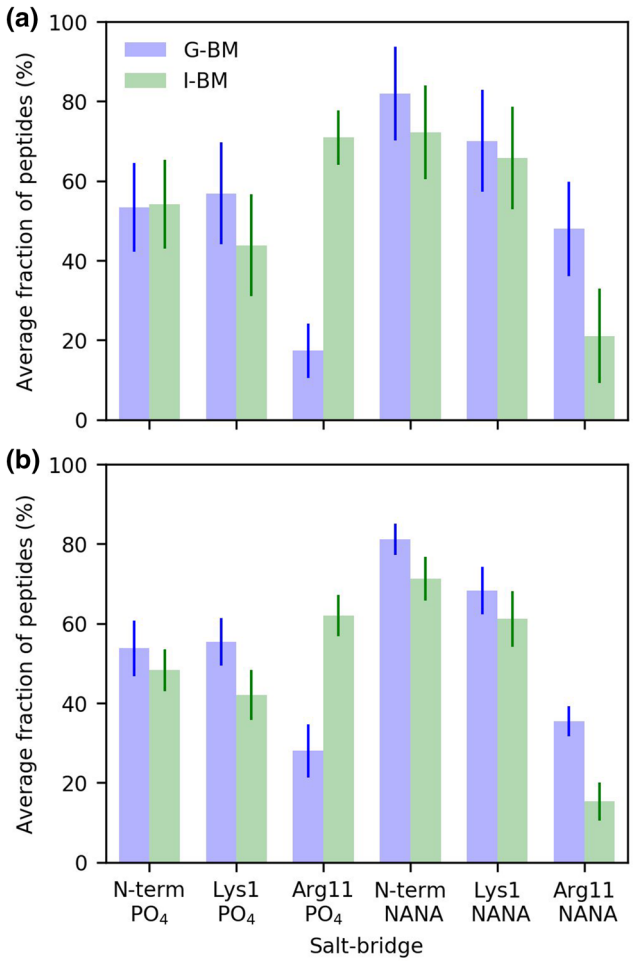

Fig. 9 Average fraction of peptides involved in salt-bridge interactions with the lipid bilayer. **a** Salt-bridge occurrence in the large CG systems **b** salt-bridge content in CG single-peptide binding simulations. A salt bridge is defined as two opposite charged beads with within 0.7 nm. The peptides found in G-BM and I-BM are shown in blue and green bars, respectively. The error bars indicate the error across simulation repeats (Color figure online)

in G-BM, which for the single-binding simulations are equally distributed between PO4 and NANA.

Interactions with NANA are dominating in both binding modes, and notably interactions between Lys1 and the *N*-terminal with NANA are the most frequent salt bridges formed in both binding modes, although Arg11–PO4 is also highly populated in I-BM (Fig. 9). Arg11 is predominantly interacting with NANA in the large systems and when found in G-BM. In contrast, Arg11 in I-BM mostly interacts with PO4. Anionic lipids are a major driving force in the membrane association of hIAPP, as shown previously with PS and PG lipids, presumably due to cationic residues of hIAPP (Jayasinghe and Langen 2005; Knight and Miranker 2004). It is therefore expected that GM3 is the primary interaction point of PC/GM3 membranes, at least in the initial

recognition. Figure 10a,b shows the evolution of the fraction of peptides forming salt-bridge interactions to NANA and PO4, respectively, during the simulations. The rapid increase in the number of peptides with salt bridging of Lys1 and the *N*-terminal, rather than Arg11, to NANA (the G-lipids) indicates that this part of the peptide is indeed what primarily drives the binding of hIAPP to the membrane in the presence of GM3 lipids.

Co-Localization of hIAPP AND GM3

HIAPP has many salt-bridge interactions with GM3 and since GM3 has a tendency to form domains in lipid membranes (Fujita et al. 2007), hIAPP can be hypothesized to be positioned on or in the vicinity of these clusters. Hence, the co-localization of hIAPP and GM3 was investigated based on a 2D-density analysis. The density maps are generated with the *gmx densmap* tool of the individual leaflets from last 0.5 µs of the simulations of the large CG system. The map is created by dividing each leaflet into an equally spaced grid with fields of 1×1 nm and counting the number of beads of each molecule type in every cell of the grid. Based on the 2D-number density maps of GM3 and protein, the areas with the highest concentration are shown in Fig. 8 for the 5 repeats of large system CG simulations, for one leaflet of each repeat. From the plots, it is clear that areas enriched with clusters of GM3 (shown in blue) also have the highest concentration of peptides (shown in red). Figure 8 also shows the tendency of forming ganglioside-enriched and ganglioside-depleted areas.

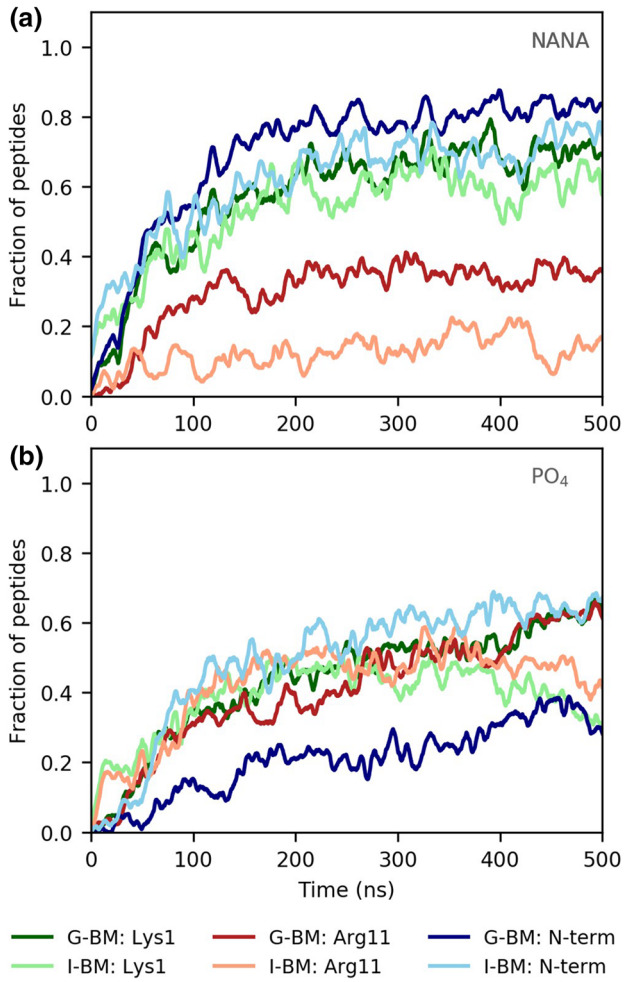

Fig. 10 Fraction of the peptides that form salt-bridge interactions with the anionic lipids over time for G-BM and I-BM. Separated in Lys1 (green), Arg11 (red), and the *N*-terminal (blue) with salt bridge interactions to **a** NANA and **b** the phospholipid phosphates (PO4). Interactions found in I-BM are displayed in lighter shades than for G-BM (Color figure online)

Umbrella Sampling

To further investigate the binding of hIAPP to a DOPC/GM3 membrane, a series of umbrella sampling simulations were conducted. The data and results are available in the Supplementary Information. The energy profiles indicated an energy minimum at lipid head groups, and both binding modes are found to be close to energy minima. The limited accuracy of the umbrella sampling for a system of this complexity especially in a coarse-grained representation makes the depth and width of the binding minima uncertain, and thus makes the two binding modes indistinguishable.

Conformational Changes

The above analyses of the binding modes of hIAPP on GM3 containing lipid bilayers were conducted with CG MD simulations. A characteristic of the Martini CG FF is that the secondary structure of proteins and peptides is constrained (Monticelli et al. 2008), which means that the secondary structure of the two helical segments of the peptide cannot change. In addition, the Martini CG FF also has a tendency to over-stabilize electrostatic interactions and thereby also potentially the peptide binding modes (Javanainen et al. 2017; Schmalhorst et al. 2017). To further investigate the conformational stability of the identified membrane-bound conformations, five structures from each of the two identified binding modes, G-BM and I-BM, were extracted randomly and converted to an atomistic resolution. Each of the resulting atomistic systems was simulated five times for 2 µs using the CHARMM22* force field for the peptides and CHARMM36 for the lipids.

The root mean square deviation (RMSD) was calculated for each repeat to assess the deformation of the peptide conformations (Fig. 11). The structures initially found in G-BM shows RMSD values on the order of 6 to 12 Å, in contrast to the structures starting from I-BM, which had lower RMSD values in the range of 3 to 8 Å. This suggests

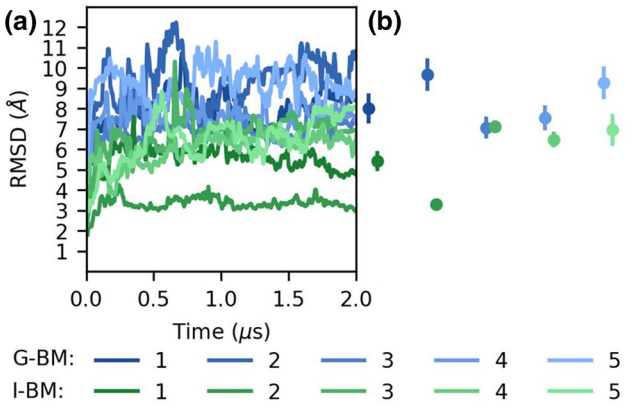

Fig. 11 Root mean square deviation plot of the atomistic simulations. The RMSD is calculated for the backbone atoms. The RMSD for the structures starting in G-BM and I-BM are shown in shades of blue and green, respectively, with each replica (1–5) in a different level of brightness. **a** Shows the RMSD development in time with a running mean using 10 ns windows, **b** shows the average value and standard deviation of the RMSD for the peptides in the last 1 μs of the simulations (Color figure online)

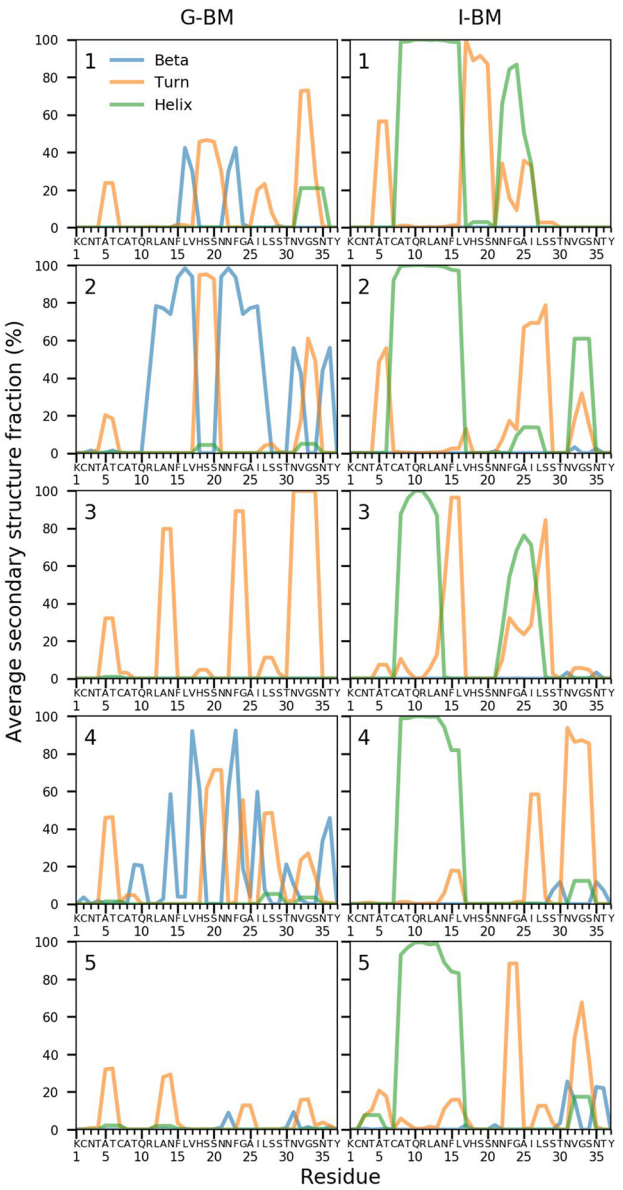

Fig. 12 Fraction of the average secondary structure content for the peptides in the last 1 μs of each repeat of the atomistic simulations. The degree of β-strand, turn, and α-helix is shown in blue, orange, and green, respectively (Color figure online)

that the structures in G-BM are not stable but I-BM may be more stable.

The secondary structure distributions of the peptides, during the last half of each of the atomistic simulations are shown in Fig. 12, as calculated with the DSSP algorithm (Kabsch and Sander 1983). It is seen that in the simulations for the peptides starting from I-BM (right column), the *N*-terminal α-helix with residues Ala8 to Leu16 is conserved throughout the simulations. In contrast, for the simulations starting from G-BM (left column), the *N*-terminal α-helix unfolds. The α-helical structure is known to be stabilized in other membrane environments, e.g., membranes containing PS lipids and in SDS micelles and to be destabilized prior to amyloid formation. The formation and stabilization of an amphiphilic helix is common for small peptides interacting with the hydrophobic/hydrophilic interface of lipid membranes (Segrest et al. 1974), as it is seen here for I-BM.

The G-BM locates the peptides at the interface between the hydrophilic head groups of the ganglioside lipids and the solution. Both of these partitions are hydrophilic, thus leaving the hydrophobic side of the helices exposed, which is a likely cause for the structural instability. Substantial β-strand content is observed in three of the repeats starting in G-BM (repeat 1, 2, and 4 in the left column). The β-sheets formed are hairpins with a turn at residues His18 to Ser20. This β-turn has been observed in several previous studies, (Dupuis et al. 2011; Reddy et al. 2010; Singh et al. 2013) and it is hypothesized to be an on-pathway intermediate in the formation of fibrils, because it has a turn similar to the currently available fibril structures, as illustrated in Fig. 2b-d. The hairpin is most likely stabilized in the solvent-exposed region by the backbone interactions and preferential interactions between the sidechains, in contrast, the amphiphilic helix was destabilized by the high concentration of exposed hydrophobic residues. To illustrate the conformational differences, examples of end structures from simulations starting from G-BM and I-BM, respectively, are shown in Fig. 13, where it is clear that β-hairpins are present for simulations starting from the G-BM (Fig. 13c, d), whereas the *N*-terminal is deeply buried in the I-BM (Fig. 13a-b).

The salt-bridge count between peptides and lipids in the atomistic simulations looks similar to that of the CG

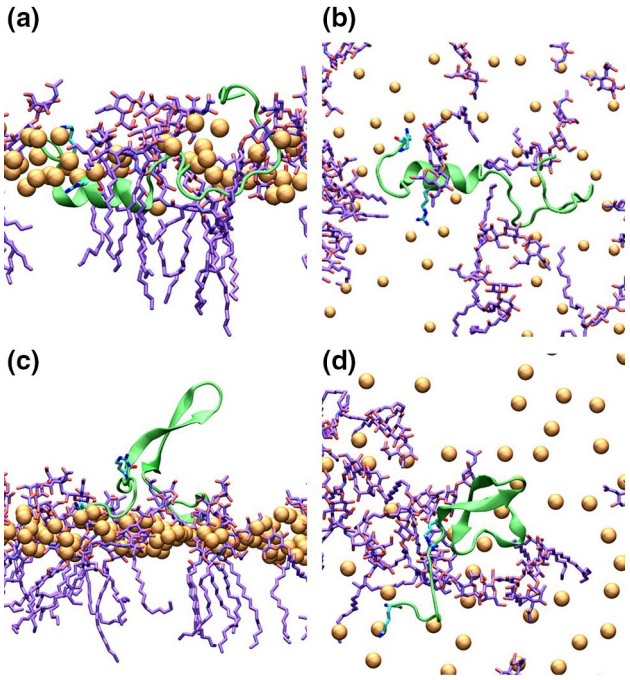

Fig. 13 End frame structures from atomistic simulations of peptides. The phospholipid phosphates are shown in orange, GM3 is shown in purple, and the peptides are shown in green **a** I-BM sideview **b** I-BM topview **c** G-BM sideview **d** G-BM topview. In I-BM (**a**, **b**) the *N*-terminal helix is clearly visible, while for G-BM (**c**, **d**) a β-hairpin is found (Color figure online)

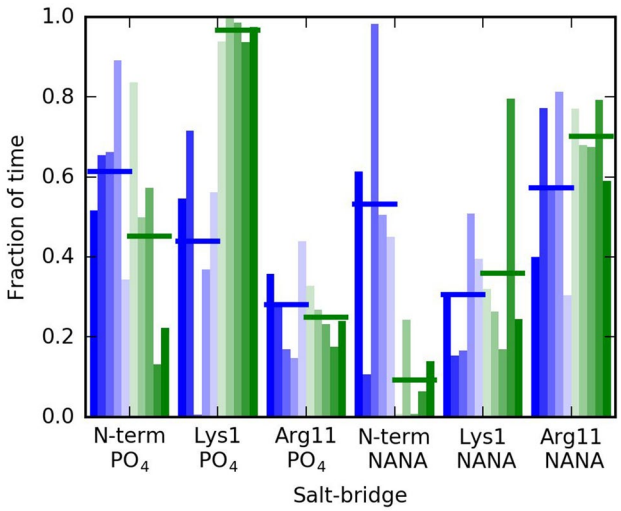

Fig. 14 Normalized salt-bridge count for the atomistic simulations of hIAPP on GM3-containing membranes. The count for the peptides starting in G-BM are shown in shades of blue and the peptides starting in I-BM are shown in shades of green. The average for each binding mode is shown with horizontal lines (Color figure online)

simulations (Fig. 14), however, the peptides are more flexible and no longer bound in two well-defined states. In the analysis of the atomistic simulations, a salt bridge is defined as two opposite charges within 5 Å (Ahmed et al. 2018). The peptides starting in I-BM are the least flexible and retain the helical structure in the *N*-terminal. All the peptides in I-BM display a salt bridge between the Lys1 sidechain and the PO4 atoms of phospholipid as an important anchor for the helix to the membrane. A major difference between the formation of salt bridges in the two binding modes is the presence of a salt bridge between the *N*-terminal of the peptides and NANA which is present at a large fraction of the time in the simulations initiated from G-BM, and almost absent in simulations initiated in I-BM.

Dual Role Of Ganglioside Lipids

From the identification of two binding modes of hIAPP at a GM3/DOPC membrane, and their properties, we propose a dual role of the gangliosides on hIAPP aggregation. We suggest that the effect of ganglioside lipids on the hIAPP aggregation rate depends on the dominating binding mode of hIAPP on the membrane, as illustrated in Fig. 15. In this study, we have used a high concentration of GM3, where the gangliosides spontaneously cluster in the membrane, to form an anionic, hydrophilic plateau raised above the phospholipids. hIAPPs are attracted to these and bind predominantly to the ganglioside domains (G-BM), which induce a conformational change towards an aggregation prone conformation (Dupuis et al. 2011; Reddy et al. 2010; Singh et al. 2013), as evidenced from the atomistic simulations.

Since the peptides are attracted to the ganglioside domains, the local peptide concentration will be high, which will most likely accelerate the aggregation process. In contrast, the peptides bound at the hydrophobic/hydrophilic

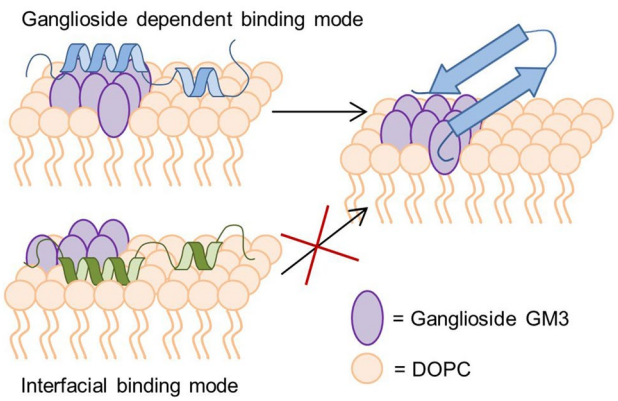

Fig. 15 Sketch of the proposed mechanism of hIAPP binding modes and conformational change of DOPC/GM3 lipid bilayers. The DOPC lipids are shown with orange head groups and GM3 is shown with purple head groups. The peptides in the two binding modes, G-BM and I-BM, are shown in blue and green, respectively (Color figure online)

interface (I-BM) in the vicinity of the gangliosides are stabilized in an α-helical conformation and since the hydrophilic side of the peptides are engaged in interactions with the ganglioside headgroups, and thus shielded from the solution, they are protected from both conformational changes and interaction with other peptides, hence slowing down oligomer formation. At low concentration, the clusters of gangliosides are small, thus yielding a large domain boundary and a small domain area. The peptides are therefore more likely to bind to interface rather than the ganglioside head groups, as in the case with a high concentration and high domain area. This mechanism is similar to what was previously proposed by Amaro et al. in the case of amyloid β (Amaro et al. 2016). Amaro et al. found that a 4% concentration of GM1 inhibited amyloid formation, whereas a 20% GM1 concentration accelerated amyloid formation (Amaro et al. 2016).

Conclusions

The strong attraction between the *N*-terminal and anionic lipids is well described for simple anionic phospholipids such as PS and PG lipids, which accelerate both amyloid formation and membrane damage at vesicles in vitro (Zhang et al. 2017). Ganglioside lipids are physiologically relevant anionic lipids, and they induce hIAPP membrane damage and amyloid formation (Wakabayashi and Matsuzaki 2009). Here, we have described in detail how hIAPP binds to ganglioside-containing membranes. Large system CG simulations of several hIAPP peptides revealed two binding modes: one at the hydrophobic/hydrophilic interface, and another on top of the ganglioside lipid head groups, as sketched in Fig. 7. Both binding modes are equally occupied with 42% of the peptides in each. The presence of two binding modes is independent of larger GM3-depleted areas and interactions between peptides as seen from 100 single-peptide binding simulations. At low GM3 concentration (4%), the binding of the peptides on the ganglioside headgroups was reduced to 10%. Electrostatic interactions between the *N*-terminal of hIAPP and the NANA of GM3 s are dominating both binding modes, which indicates that this carries the major responsibility for the affinity of hIAPP towards ganglioside lipids (Figs. 9, 10). In the large systems, hIAPP and GM3 show a tendency to co-localize on the membrane (Fig. 8).

Atomistic simulations of peptides starting from the two binding modes indicated that the hydrophobic/hydrophilic interface stabilized the α-helical conformations, whereas the ganglioside head groups induced transition to conformations of random coil and β-hairpins. The observed mechanism is sketched in Fig. 15. A similar mechanism was observed for Aβ interacting with ganglioside-containing membranes (Manna and Mukhopadhyay 2013). Whether the transition to a β-hairpin is merely on-pathway to fibril structures, cytotoxic oligomers, or both, is however still unknown, but β-hairpins are often observed on the pathway to oligomerization in simulations, and β-hairpins can also be observed experimentally by trapping soluble hIAPP in β-wrap proteins (Mirecka et al. 2016). We propose that the concentration-dependent dual role of ganglioside lipids on Aβ aggregation observed by Amaro et al. (2016) is also valid for hIAPP due to the presence of two binding modes and with the high concentration of ganglioside lipids inducing conformation changes. This hypothesis however needs further experimental validation in vitro, for example, by using ThT fluorescence to study the effect of ganglioside concentration on the kinetics of hIAPP amyloid formation.

Further studies are on the way in our group that focus on the role of microdomains and cholesterol on the membrane interactions of hIAPP, which will lead to more detailed insight into the aggregation process in a physiologically relevant setting.

Acknowledgments Computations were performed at the Grendel cluster of the Centre for Scientific Computing Aarhus (CSCAA), Aarhus University and at the Abacus 2.0 of the DeIC National HPC Centre, University of Southern Denmark. Dr. Xavier Periole is thanked for fruitful discussions.

Funding Funding was provided by Lundbeckfonden (Grant No. R191-2015-827) and by Sino-Danish Center.

Compliance with Ethical Standards

Conflict of interest The authors declare no conflicts of interest.

Research Involving Human and Animal Participants This article does not contain any studies with human participants or animals performed by any of the authors.

Informed Consent All co-authors have agreed to submission and we state that the results have neither previously been made publicly available, nor are they under consideration for publication elsewhere.

References

Abraham MJ, Murtola T, Schulz R, Páll S, Smith JC, Hess B, Lindahl E (2015) GROMACS: high performance molecular simulations through multi-level parallelism from laptops to supercomputers. SoftwareX 1–2:19–25

Ahmed MC, Papaleo E, Lindorff-Larsen K (2018) How well do force fields capture the strength of salt bridges in proteins? PeerJ 6:e4967

Amaro M, Šachl R, Aydogan G, Mikhalyov II, Vácha R, Hof M (2016) GM1 ganglioside inhibits β-amyloid oligomerization induced by sphingomyelin. Angew Chem Int Ed 55:9411–9415

Anguiano M, Nowak RJ, Lansbury PT (2002) Protofibrillar islet amyloid polypeptide permeabilizes synthetic vesicles by a pore-like mechanism that may be relevant to type II diabetes. Biochemistry 41:11338–11343

Berendsen HJC, Postma JP, van Gunsteren WF, DiNola A, Haak JR (1984) Molecular dynamics with coupling to an external bath. J Chem Phys 81:3684–3690

Bussi G, Donadio D, Parrinello M (2007) Canonical sampling through velocity rescaling. J Chem Phys 126:014101

Caillon L, Lequin O, Khemtémourian L (2013) Evaluation of membrane models and their composition for islet amyloid polypeptide-membrane aggregation. Biochimica et Biophysica Acta (BBA)-Biomembranes 1828:2091–2098

Calamai M, Pavone FS (2013) Partitioning and confinement of GM1 ganglioside induced by amyloid aggregates. FEBS Lett 587:1385–1391

de Jong DH et al (2013) Improved parameters for the martini coarse-grained protein force field. J Chem Theory Comput 9:687–697

Dotta F et al (1989) Ganglioside expression in human pancreatic islets. Diabetes 38:1478–1483

Dupuis NF, Wu C, Shea JE, Bowers MT (2011) The amyloid formation mechanism in human IAPP: dimers have β-strand monomer-monomer interfaces. J Am Chem Soc 133:7240–7243

Engel MFM et al (2008) Membrane damage by human islet amyloid polypeptide through fibril growth at the membrane. Proc Natl Acad Sci USA 105:6033–6038

Essmann U, Perera L, Berkowitz ML, Darden T, Lee H, Pedersen LG (1995) A smooth particle mesh Ewald method. J Chem Phys 103:8577–8593

Fu L, Wang Z, Batista VS, Yan ECY (2015) New insights from sum frequency generation vibrational spectroscopy into the interactions of islet amyloid polypeptides with lipid membranes. J Diabetes Res. https://doi.org/10.1155/2016/7293063

Fujita A, Cheng J, Hirakawa M, Furukawa K, Kusunoki S, Fujimoto T (2007) Gangliosides GM1 and GM3 in the living cell membrane form clusters susceptible to cholesterol depletion and chilling. Mol Biol Cell 18:2112–2122

Gu R-X, Ingólfsson HI, DeVries AH, Marrink SJ, Tieleman DP (2016) Ganglioside-lipid and ganglioside-protein interactions revealed by coarse-grained and atomistic molecular dynamics simulations. J Phys Chem B 121(15):3262–3275

Hess B, Bekker H, Berendsen HJC, Fraaije JGEM (1997) LINCS: a linear constraint solver for molecular simulations. J Comput Chem 18:1463–1472

Hockney RW, Goel SP, Eastwood JW (1974) Quiet high-resolution computer models of a plasma. J Comput Phys 14:148–158

Hoffmann KQ, McGovern M, Chiu CC, de Pablo JJ (2015) Secondary structure of rat and human amylin across force fields. PLoS ONE 10:e0134091

Hoover WG (1985) Canonical dynamics: equilibrium phase-space distributions. Phys Rev A: At, Mol, Opt Phys 31:1695–1697

Höppener JWM, Ahrén B, Lips CJM (2000) Islet amyloid and type 2 diabetes mellitus. N Engl J Med 343:411–419

Javanainen M, Martinez-Seara H, Vattulainen I (2017) Excessive aggregation of membrane proteins in the Martini model. PLoS ONE 12:e0187936

Jayasinghe SA, Langen R (2005) Lipid membranes modulate the structure of islet amyloid polypeptide. Biochemistry 44:12113–12119

Jayasinghe SA, Langen R (2007) Membrane interaction of islet amyloid polypeptide. Biochimica et Biophysica Acta (BBA)-Biomembranes 1768:2002–2009

Jurgens CA et al (2011) β-cell loss and β-cell apoptosis in human type 2 diabetes are related to islet amyloid deposition. Am J Pathol 178:2632–2640

Kabsch W, Sander C (1983) Dictionary of protein secondary structure: pattern recognition of hydrogen-bonded and geometrical features. Biopolymers 22:2577–2637

Khemtémourian L, Doménech E, Doux JPF, Koorengevel MC, Killian JA (2011) Low pH acts as inhibitor of membrane damage induced by human islet amyloid polypeptide. J Am Chem Soc 133:15598–15604

Knight JD, Miranker AD (2004) Phospholipid catalysis of diabetic amyloid assembly. J Mol Biol 341:1175–1187

Knight JD, Hebda JA, Miranker AD (2006) Conserved and cooperative assembly of membrane-bound α-helical states of islet amyloid polypeptide. Biochemistry 45:9496–9508

Knight JD, Williamson JA, Miranker AD (2008) Interaction of membrane-bound islet amyloid polypeptide with soluble and crystalline insulin. Protein Sci 17:1850–1856

Koldsø H, Shorthouse D, Hélie J, Sansom MSP (2014) Lipid clustering correlates with membrane curvature as revealed by molecular simulations of complex lipid bilayers. PLoS Comput Biol 10:e1003911

Last NB, Rhoades E, Miranker AD (2011) Islet amyloid polypeptide demonstrates a persistent capacity to disrupt membrane integrity. Proc Natl Acad Sci USA 108:9460–9465

Laude AJ, Prior IA (2004) Plasma membrane microdomains: organization, function and trafficking. Mol Membr Biol 21:193–205

Lee C-C, Sun Y, Huang HW (2012) How type II diabetes-related islet amyloid polypeptide damages lipid bilayers. Biophys J 102:1059–1068

Lemkul JA, Bevan DR (2011) Lipid composition influences the release of Alzheimer's amyloid β-peptide from membranes. Protein Sci 20:1530–1545

López CA, Sovova Z, van Eerden FJ, de Vries AH, Marrink SJ (2013) Martini force field parameters for glycolipids. J Chem Theory Comput 9:1694–1708

Luca S, Yau W-M, Leapman R, Tycko R (2007) Peptide conformation and supramolecular organization in amylin fibrils: constraints from solid-state NMR. Biochemistry 46:13505–13522

Lukinius A, Wilander E, Westermark GT, Engstrom U, Westermark P (1989) Co-localization of islet amyloid polypeptide and insulin in the b cell secretory granules of the human pancreatic-islets. Diabetologia 32:240–244

Lutz TA (2012) Control of energy homeostasis by amylin. Cell Mol Life Sci 69:1947–1965

Maloy AL, Longnecker DS, Robert Greenberg E (1981) The relation of islet amyloid to the clinical type of diabetes. Hum Pathol 12:917–922

Manna M, Mukhopadhyay C (2013) Binding, conformational transition and dimerization of amyloid-β peptide on GM1-containing ternary membrane: insights from molecular dynamics simulation. PLoS ONE 8:e71308

Marrink SJ, de Vries AH, Mark AE (2004) Coarse grained model for semiquantitative lipid simulations. J Phys Chem B 108:750–760

Marrink SJ, Risselada HJ, Yefimov S, Tieleman DP, de Vries AH (2007) The MARTINI force field: coarse grained model for biomolecular simulations. J Phys Chem B 111:7812–7824

Mirecka EA, Feuerstein S, Gremer L, Schröder GF, Stoldt M, Willbold D, Hoyer W (2016) β-Hairpin of islet amyloid polypeptide bound to an aggregation inhibitor. Sci Rep 6:33474

Mirzabekov TA, Lin MC, Kagan BL (1996) Pore formation by the cytotoxic islet amyloid peptide amylin. J Biol Chem 271:1988–1992

Mocchetti I (2005) Exogenous gangliosides, neuronal plasticity and repair, and the neurotrophins. Cell Mol Life Sci 62:2283–2294

Monticelli L, Kandasamy SK, Periole X, Larson RG, Tieleman DP, Marrink S-J (2008) The MARTINI coarse-grained force field: extension to proteins. J Chem Theory Comput 4:819–834

Nanga RPR, Brender JR, Vivekanandan S, Ramamoorthy A (2011) Structure and membrane orientation of IAPP in its natively amidated form at physiological pH in a membrane environment. Biochimica Et Biophysica Acta-Biomembranes 1808:2337–2342

Páll S, Hess B (2013) A flexible algorithm for calculating pair interactions on SIMD architectures. Comput Phys Commun 184:2641–2650

Parrinello M, Rahman A (1981) Polymorphic transitions in single crystals: a new molecular dynamics method. J Appl Phys 52:7182–7190
Periole X (2013) Is it possible to calculate salt-bridges in Martini? http://www.cgmartini.nl/index.php/component/kunena/10-other/1459-is-it-possible-to-calculate-salt-bridges-in-martini. Accessed 13 Jan 2019
Piana S, Lindorff-Larsen K, Shaw David E (2011) How robust are protein folding simulations with respect to force field parameterization? Biophys J 100:L47–L49
Quist A et al (2005) Amyloid ion channels: a common structural link for protein-misfolding disease. Proc Natl Acad Sci USA 102:10427–10432
Reddy AS et al (2010) Stable and metastable states of human amylin in solution. Biophys J 99:2208–2216
Saito M, Ito M, Sugiyama K (1999) A specific loss of c-series gangliosides in pancreas of streptozotocin-induced diabetic rats. Life Sci 64:1803–1810
Sasahara K, Hall D, Hamada D (2010) Effect of lipid type on the binding of lipid vesicles to islet amyloid polypeptide amyloid fibrils. Biochemistry 49:3040–3048
Sasahara K, Morigaki K, Okazaki T, Hamada D (2012) Binding of islet amyloid polypeptide to supported lipid bilayers and amyloid aggregation at the membranes. Biochemistry 51:6908–6919
Scalisi S, Sciacca MFM, Zhavnerko G, Grasso DM, Marletta G, La Rosa C (2010) Self-assembling pathway of hIAPP fibrils within lipid bilayers. ChemBioChem 11:1856–1859
Schmalhorst PS, Deluweit F, Scherrers R, Heisenberg C-P, Sikora M (2017) Overcoming the limitations of the MARTINI force field in simulations of polysaccharides. J Chem Theory Comput 13:5039–5053
Segrest JP, Jackson RL, Morrisett JD, Gotto AM (1974) A molecular theory of lipid—protein interactions in the plasma lipoproteins. FEBS Lett 38:247–253
Singh S, Chiu C-c, Reddy AS, de Pablo JJ (2013) α-Helix to β-hairpin transition of human amylin monomer. J Chem Phys 138:155101
Sparr E et al (2004) Islet amyloid polypeptide-induced membrane leakage involves uptake of lipids by forming amyloid fibers. FEBS Lett 577:117–120
Steinbach PJ, Brooks BR (1994) New spherical-cutoff methods for long-range forces in macromolecular simulation. J Comput Chem 15:667–683
Stumvoll M, Goldstein BJ, van Haeften TW (2007) Pathogenesis of type 2 diabetes. Endocr Res 32:19–37
Terzi E, Hölzemann G, Seelig J (1997) Interaction of Alzheimer β-amyloid peptide (1–40) with lipid membranes. Biochemistry 36:14845–14852
Tironi IG, Sperb R, Smith PE, van Gunsteren WF (1995) A generalized reaction field method for molecular dynamics simulations. J Chem Phys 102:5451–5459
Wahlström A, Hugonin L, Perálvarez-Marín A, Jarvet J, Gräslund A (2008) Secondary structure conversions of Alzheimer's Aβ (1–40) peptide induced by membrane-mimicking detergents. FEBS J 275:5117–5128
Wakabayashi M, Matsuzaki K (2009) Ganglioside-induced amyloid formation by human islet amyloid polypeptide in lipid rafts. FEBS Lett 583:2854–2858
Wassenaar TA, Pluhackova K, Böckmann RA, Marrink SJ, Tieleman DP (2014) Going backward: a flexible geometric approach to reverse transformation from coarse grained to atomistic models. J Chem Theory Comput 10:676–690
Wassenaar TA, Ingólfsson HI, Böckmann RA, Tieleman DP, Marrink SJ (2015) Computational lipidomics with insane: a versatile tool for generating custom membranes for molecular simulations. J Chem Theory Comput 11:2144–2155
Westermark P (1995) Islet amyloid polypeptide and amyloid in the islets of Langerhans. In: Leslie RDG, Robbins D (eds) Diabetes: clinical science in practice. Cambridge Univ. Press, Cambridge, pp 189–199
Westermark P, Andersson A, Westermark GT (2011) Islet amyloid polypeptide, islet amyloid, and diabetes mellitus. Physiol Rev 91:795–826
Wilcox G (2005) Insulin and insulin resistance. Clin Biochem Rev 26:19–39
Williamson JA, Miranker AD (2007) Direct detection of transient α-helical states in islet amyloid polypeptide. Protein Sci 16:110–117
Williamson JA, Loria JP, Miranker AD (2009) Helix stabilization precedes aqueous and bilayer-catalyzed fiber formation in islet amyloid polypeptide. J Mol Biol 393:383–396
Yesylevskyy SO, Schäfer LV, Sengupta D, Marrink SJ (2010) Polarizable water model for the coarse-grained MARTINI force field. PLoS Comput Biol 6:e1000810
Zhang X, St Clair JR, London E, Raleigh DP (2017) Islet amyloid polypeptide membrane interactions: effects of membrane composition. Biochemistry 56:376–390
Zhao HL, Lai FMM, Tong PCY, Zhong DR, Yang D, Tomlinson B, Chan JCN (2003) Prevalence and clinicopathological characteristics of islet amyloid in chinese patients with type 2 diabetes. Diabetes 52:2759–2766

Affiliations

Mikkel Christensen[1,2] · Birgit Schiøtt[1]

[1] Interdisciplinary Nanoscience Center (iNANO) and Department of Chemistry, Aarhus University, Langelandsgade 140, 8000 Aarhus, Denmark

[2] Sino-Danish Center for Education and Research, Aarhus, Denmark